Colloid Polym Sci (2006) 284: 1303–1311
DOI 10.1007/s00396-006-1516-5

ORIGINAL CONTRIBUTION

M. Ballauff
A. Jusufi

Anomalous small-angle X-ray scattering: analyzing correlations and fluctuations in polyelectrolytes

Received: 17 March 2006
Accepted: 21 April 2006
Published online: 24 May 2006

M. Ballauff (✉) · A. Jusufi
Physikalische Chemie I,
University of Bayreuth,
95440 Bayreuth, Germany
e-mail: matthias.ballauff@uni-bayreuth.de

Abstract We review recent structural investigations done by anomalous small-angle X-ray scattering (ASAXS). ASAXS uses the dependence of the scattering length of a given element if the energy of the incident X-ray beam is near the absorption edge of this element. The analysis of the ASAXS data leads to three partial intensities. We show that the comparison of these three partial intensities leads to valuable information in fluctuating systems. This has been demonstrated from data derived from recent molecular dynamics simulations of charged colloidal spheres. Moreover, it is shown that the three partial intensities can be obtained from experimental ASAXS data indeed. As an example for this analysis, we discuss recent ASAXS data referring to rod-like polyelectrolytes. These polyelectrolytes consist of a stiff poly(p-phenylene) backbone with attached charged groups that are balanced by bromine counterions. The three partial intensities can be determined experimentally and compared to the prediction of the Poisson–Boltzmann cell model. Quantitative agreement is found demonstrating the strong correlation of the counterions to the rod-like macroion. ASAXS is thus shown to furnish information not available by the conventional small-angle scattering experiment.

Keywords Polyelectrolyte · ASAXS · SAXS · Counterion condensation

Introduction

Charged colloidal systems consist of a highly charged macroion and a concomitant number of counterions [1, 2]. Immersed in water or another solvent with a high dielectric constant, the counterions will dissociate. Examples are given by polyelectrolytes as, e.g., DNA or by charged micellar systems. A central question in this field is the correlation of the dissociated counterions to the macroion, which has been reviewed recently [3–6]. A part of the counterions will be strongly correlated if the macroion is characterized by a sufficiently high charge density. The "counterion condensation" thus induced in highly charged linear polyelectrolytes has been the subject of numerous investigations recently [7, 8]. In case of star polyelectrolytes or spherical polyelectrolyte brushes, this correlation is even more pronounced [9–11]. Clearly, the question arises whether this correlation can be described in terms of a meanfield-type model that neglects correlated fluctuations, or whether these fluctuations must be taken into account for an appropriate description of the system.

In principle, small-angle X-ray scattering (SAXS) is well suited to investigate the spatial correlation of the counterions to the macroion [12, 13]. The data thus obtained may directly be compared to the predictions based on a meanfield ansatz. Moreover, SAXS is sensitive towards contributions that stem from fluctuations of the counterions. However, a meaningful comparison to the predictions of theory requires the decomposition of the measured intensity $I(q)$ $[q = (4\pi/\lambda)\sin(\theta/2)]$ (q is the magnitude of scattering vector; λ is the wave length of the X-ray beam; θ is the scattering vector) into partial intensities that give the separate contributions of the macroion and the counterions, respectively. In conventional SAXS experi-

ments, this information can only be obtained through the exchange of counterions that differ widely in scattering length [14–16]. Small-angle neutron scattering (SANS) provides an alternative because sufficient contrast can be achieved through the use of deuterated counterions [17]. However, the exchange of counterions or bulky hydrophobic counterions to be used in SANS experiments may lead to specific effects that may become as important as electrostatic interaction [1, 2].

Many years ago, Stuhrmann showed that anomalous dispersion can circumvent this problem in studies of polyelectrolytes by SAXS [18, 19]. This method utilizes the dependence of the scattering factor f if the energy of the incident radiation is near the absorption edge of the counterions [19]. Hence, the scattering factor f_{ion} becomes a complex function of the energy E of the incident radiation near the absorption edge of the ions [18, 19]:

$$f_{ion} = f_0 + f'(E) + \tilde{i} f''(E) \tag{1}$$

The first term, f_0 , is the nonresonant term, which equals the atomic number of the element [12, 20]. The second and third terms in Eq. 1 are the real and the imaginary part due to the anomalous dispersion near the absorption edge, and $\tilde{i}$ is the complex unit. The imaginary part, $f''(E)$, is directly related to the absorption cross section for X-rays of energy E . The respective scattering lengths are obtained by the multiplication of these quantities by the Thomson factor r_0 [13, 18]. Figure 1 displays the scattering factors thus defined as the function of the energy E of the incident radiation. With the aid of synchrotron radiation, the energy of the incident beam can be tuned to the absorption edge of, e.g., rubidium or bromide counterions.

Here, we consider the application of anomalous small-angle X-ray scattering (ASAXS) to the analysis of polyelectrolytes in solution. To demonstrate the power of this method, we discuss the partial intensities in detail and show that they contain different information. As an example, we shall discuss the application of ASAXS to solutions of rod-like polyelectrolytes in solution [23–26]. Here, it will become obvious that the three partial intensities can be obtained from experimental data in good accuracy. The same analysis has recently been applied to spherical polyelectrolyte brushes [27]. Moreover, Goerigk et al. presented the first analysis of flexible polyelectrolytes in the presence of strontium ions [28]. Hence, recent work has established ASAXS as the method of choice for the analysis of polyelectrolytes in solution.

Moreover, we could show recently that ASAXS furnishes information on fluctuating systems that is not available by a conventional SAXS experiment [29, 30]. This analysis is based on molecular dynamics (MD) simulations and demonstrates that fluctuating contributions can be distinguished from the ASAXS-data. Here, we wish to review this approach and its usefulness by application to data obtained from rod-like polyelectrolytes [25]. There is

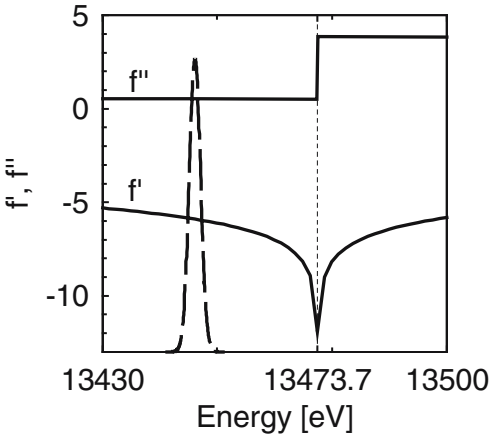

Fig. 1 Dependence of the effective scattering factors f'_{eff} and f''_{eff} of bromine on the energy E of the incident X-ray beam. The scattering factor f' taken from Henke et al. and Brennan and Cowan [21, 22] is plotted against the energy of the incident beam. The energy of the edge is marked by a *dashed line*. The breadth of the energy distribution of the primary beam is approximated by a Gaussian and given by a *dash-dotted line*. The finite width of the primary beam imposes no problem unless the experiment is done in the immediate neighborhood of the edge. Then the effective scattering factors f'_{eff} and f''_{eff} result from a convolution of the energy spread of the primary beam with f' or f'', respectively [25, 27]

no doubt that the same type of analysis can be applied to other systems in which one component exhibits an anomalous dispersion (see Eq. 1). Examples are given, e.g., by metallic nanoparticles dispersed in catalysts [31–33], alloys [34], or other composite materials [35]. The usual analysis of ASAXS intensities obtained from these systems leads only to two intensities. It will become apparent from the present discussion that the underlying simplifications are unnecessary and may even lead to questionable conclusions.

Theory

ASAXS: partial intensities

The scattering intensity originating from a solution of dissolved objects can be rendered as [13, 20]

$$I(q) = \frac{N}{V} I_0(q) S(q) \tag{2}$$

Here, N/V is the number of the dissolved polyelectrolyte molecules per volume, whereas $I_0(q)$ denotes the scattering intensity of an isolated macromolecule. $S(q)$ is the effective structure factor that takes into account the effect of finite concentrations. Here, we shall disregard the influence of $S(q)$ because we only consider dilute

solutions. A more detailed discussion of $S(q)$ is given by Dingenouts et al. [27].

The charged colloid or polyelectrolyte under consideration here consists of a macroion and the respective number of counterions. We assume that only the counterions have an anomalous contribution according to Eq. 1. For ions immersed in a medium with electron density ρ_s, the number of excess electrons per ion is [23–25]

$$\Delta f_{ion} = f_{ion} - \rho_s V_{ion} \tag{3}$$

where V_{ion} is the volume of a single ion. The quantity f_0 hence denotes the scattering contribution of a single counterion that is independent of the energy of the incident radiation. In the same way, the contrast of the macroion is given by $\Delta f_m = f_m - \rho_s V_m$, where f_m is the scattering factor of the macroion and V_m is its volume.

The resulting scattering cross section follows as

$$I_0(q) = F(q)\, F^*(q) \tag{4}$$

where $F(q)$ denotes the scattering amplitude. Because of the complex scattering length densities of the counterions, $F(q)$ is a complex function in general. It may be decomposed of a nonresonant part, $F_0(q)$, and a resonant part, $F_{res}(q)$:

$$F(q) = F_0(q) + F_{res}(q) \tag{5}$$

The resonant contribution contains the scattering amplitude $v(q)$ of the counterions only:

$$F_{res}(q) = (f'(E) + \tilde{i}\, f''(E))v(q) \tag{6}$$

Given the scattering length by Eq. 1, and using Eqs. 5 and 6 in the definition of $I_0(q)$, $I_0(q)$ follows as [18, 25, 27]

$$\begin{aligned} I_0(q) =& F_0^2(q) + 2f'(E)F_0(q)v(q) + \\ &+ (f'(E)^2 + f''(E)^2)v^2(q). \end{aligned} \tag{7}$$

Equation 7 shows that the intensity measured near the absorption edge consists of three ASAXS parts: The term $F_0^2(q)$ denotes the nonresonant intensity that is measured far away from the edge by the conventional SAXS experiment. The second term is the cross term of the nonresonant and resonant amplitudes of the macroion and the counterions, $F_0(q)$ and $v(q)$, respectively. The third term describes the counterion's self-contribution. Note that all terms represent ensemble averages and can be measured separately [25, 27].

Equation 7 is fully general and applies to any analysis by ASAXS. Usually, the evaluation of the data is done by subtracting two intensities $I(q)$ from each other that have been measured at two different energies of the incident beam. The third partial intensity is neglected in this analysis and the second term, namely, $F(q)v(q)$, is assigned to the anomalous scattering moieties of the sample. This may be questionable inasmuch as this term is not an intensity, but the product of two different amplitudes (see the discussion of this point by Jusufi and Ballauff [29, 30]). Under certain circumstances, $F(q)v(q)$ may even become negative! Only the third term qualifies as an intensity in the usual sense; that is, this term is the square of the amplitude of the resonant scatterers. We shall explore this important difference in more detail here.

Correlations measured by ASAXS

To discuss the information embodied in the partial intensities of an ASAXS experiment, we consider the most simple case, namely, a spherical macroion and its counterions [29]. Figure 2 gives all relevant correlations to be determined by a scattering experiment. In the following, we give a brief discussion of these terms and their relation to the experimental ASAXS data [29].

The partial intensities $\hat{g}_{\mu\nu}(q)$ are directly related to the Fourier transform of the corresponding radial pair correlation functions $g_{\mu\nu}(r) \sim \int dr'^3 \langle \rho_\mu(r+r')\rho_\nu(r')\rangle$, with $\rho_\nu(r)$ being the density distribution of particle species $\nu = m, c$ (m represents monomers; c represents counterions) [36]. We have

$$\begin{aligned} \hat{g}_{\mu\nu}(q) &= \int dr^3\, g_{\mu\nu}(r)\, \exp(-\tilde{i}qr) \\ &\sim \langle \hat{\rho}_\mu(q)\, \hat{\rho}_\nu^*(q)\rangle, \end{aligned} \tag{8}$$

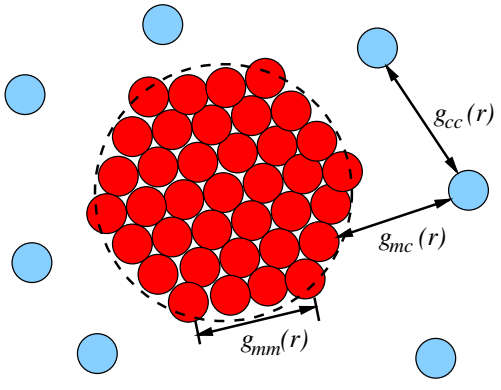

Fig. 2 Sketch of a spherical macroion surrounded by counterions. The macroion is considered to consist of homogeneously distributed monomers. The partial pair distribution functions among all particles are depicted. They illustrate the occurrence of three partial scattering contributions. See "Correlations measured by ASAXS" [29] for further details

$\hat{\rho}_\nu(q)$ is the Fourier transform of the density distribution $\rho_\nu(r)$. In what is to follow, $\langle \ldots \rangle$ denotes statistical–mechanical averages. It is important that this expression differs from the meanfield approximation (MFA) for calculations of scattering functions:

$$\hat{g}_{\mu\nu}(q) \sim \langle \hat{\rho}_\mu(q) \rangle \langle \hat{\rho}_\nu(q) \rangle. \tag{9}$$

A comprehensive discussion of both equations is also given by Harreis et al. [37].

The Fourier components $\hat{\rho}_\nu(q)$ enter into the non-resonant and resonant scattering amplitudes, $F_0(q)$ in Eq. 5 and $F_{res}(q)$ in Eq. 6, respectively [27, 29]:

$$F_0(q) = \Delta f_m \, \hat{\rho}_m(q) + \Delta f_0 \, \hat{\rho}_c(q) \tag{10}$$

$$F_{res}(q) = (f'(E) + \tilde{i} f''(E)) \, \hat{\rho}_c(q) \tag{11}$$

As a consequence, the cross section $I_0(q)$ can now be split up into the corresponding partial scattering contributions of the macroion, $\hat{g}_{mm}(q)$, of the counterions, $\hat{g}_{cc}(q)$, and of their cross-correlated scattering function, $\hat{g}_{mc}(q)$ [29]:

$$F_0^2(q) = N_m \, \Delta f_m^2 \, \hat{g}_{mm}(q) + \tag{12}$$

$$+2 (N_m + N_c) \, \Delta f_m \, \Delta f_0 \, \hat{g}_{mc}(q) + N_c \, \Delta f_0^2 \, \hat{g}_{cc}(q);$$

$$\begin{aligned} F_0(q) \, v(q) = &(N_c + N_m) \, \Delta f_m \, \hat{g}_{mc}(q) \\ &+ N_c \, \Delta f_0 \, \hat{g}_{cc}(q); \end{aligned} \tag{13}$$

$$v^2(q) = N_c \, \hat{g}_{cc}(q), \tag{14}$$

where N_m is the number of scattering particles in the macroion and N_c is the number of counterions. In this way, the three terms enumerated in Eq. 7 can be related to the three partial pair correlation functions $\hat{g}_{\mu\nu}(q)$. Thus, given the three partial intensities of Eq. 7, the evaluation of the $\hat{g}_{\mu\nu}(q)$ and the underlying $\hat{\rho}_\nu(q)$ becomes possible.

We first discuss the cross correlation $\hat{g}_{mc}(q)$ and its meaning. Experimentally, $\hat{g}_{mc}(q)$ can be obtained by subtracting Eq. 14 from Eq. 13, which leads to:

$$\hat{g}_{mc}(q) = \frac{F_0(q) v(q) - \Delta f_0 \, v^2(q)}{\Delta f_m \, (N_c + N_m)}. \tag{15}$$

In simulations, $\hat{g}_{mc}(q)$ can be directly calculated via Eq. 8. Because the macroion has a fixed shape, $\hat{\rho}_m(q)$ can be taken out from the average in Eq. 8, yielding

$$\hat{g}_{mc}(q) = \frac{2}{N_m + N_c} \, \hat{\rho}_m(q) \, \langle \hat{\rho}_c(q) \rangle. \tag{16}$$

This expression directly relates the cross-correlation $\hat{g}_{mc}(q)$ to an MFA of the density distribution of the counterions, even if the counterions are strongly fluctuating [29]. In fluctuating systems, the MFA could not be applied to the self-correlation $\hat{g}_{cc}(q)$ (compare Eqs. 8 and 9). This means that, in general, we have $\langle \hat{\rho}_\mu(q) \hat{\rho}_\nu^*(q) \rangle \neq \langle \hat{\rho}_\mu(q) \rangle \langle \hat{\rho}_\nu(q) \rangle$. However, Eq. 16 demonstrates that for colloidal systems with rigid macroions, the cross-correlation $\hat{g}_{mc}(q)$ yields the meanfield density distribution of the counterions, irrespective of any fluctuation effects of the counterions.

In conclusion, the foregoing section has clearly shown that the cross term $F_0(q)v(q)$ embodies different information than the self-term $v^2(q)$. The cross term can be used to obtain the meanfield part of the correlation of the counterion to the macroion. In contrast to this, $v^2(q)$ also carries along all the fluctuations that come into play for weakly coupled systems. Evidently, a comparison of both terms with a meanfield theory can reveal whether fluctuations are important or not. This will be shown in the subsequent section using rod-like polyelectrolytes as an example.

It is interesting to note that $\hat{g}_{mc}(q)$ can become negative because it is the product out of two different amplitudes. Oscillations in $\hat{g}_{mc}(q)$ become more pronounced if the spatial distributions of the counterions possess significant spatial variation. This has been demonstrated by a recent discussion using MD simulations [29, 30].

Example: rod-like polyelectrolytes

Up to now, only a few cases of a full analysis of polyelectrolytes by ASAXS are available in literature [25, 27, 28]. Rather than reviewing all data obtained so far, we here focus on a recent analysis of rod-like polyelectrolytes by Patel et al. [25]. The reason for this choice is given by the fact that an analytical meanfield theory for the distribution of the counterions is available. Therefore, a full comparison of theory and experiment can be done in this case. The general conclusions drawn from this analysis, however, hold for all other systems as well.

If a sufficiently high number of charges per unit length are affixed to a polymeric chain, a highly charged macroion results [1, 2]. As a consequence of this, the electrostatic energy of a counterion near to such a polyelectrolyte is high, as compared to $k_B T$. Therefore, there will be a strong correlation of a part of the counterions to the macroion. For linear rod-like polyelectrolytes, this problem has been treated already by Fuoss and coworkers [38] and by Alfrey

and coworkers [39] more than 50 years ago by introducing the Poisson–Boltzmann (PB) cell model [40]. Later, Manning introduced the notion of counterion condensation to describe this marked correlation [7].

In general, a linear polyelectrolyte is characterized by its charge parameter ξ [1, 2, 40]

$$\xi = \frac{\lambda_B}{b} \tag{17}$$

where b is the distance per unit charge and λ_b is the Bjerrum length given by $\lambda_b = e^2/4\pi\varepsilon_0\varepsilon k_B T$ (e is the unit charge; ε is the dielectric constant of the medium; and ε_0, k_B, and T have the usual meanings) [1, 3, 40]. If $\xi < 1$, the electrostatic attraction is weak as compared to the thermal energy and the Debye–Hückel approach is sufficient. However, if $\xi > 1$, counterion condensation sets in and the activity of the counterions will be strongly reduced [8].

The ASAXS data discussed here [25] have been obtained using the polyelectrolyte; the chemical structure of which is shown in Fig. 3. The macroion has a high persistence length and can be approximated by a rigid rod in excellent approximation. For such cylindrical objects in which the scattering length density varies only along the radial distance termed r_c, $I_0(q)$ follows as [13]

$$I_0\,(q) = \int_0^1 F(q,\alpha)F^*(q,\alpha)d\alpha \tag{18}$$

where α is the cosine of the angle between the $\vec{q}$ and $\vec{z}$. Here, $\vec{z}$ denotes the unit vector along the long axis of the rod. For rods of length L, it is given by [13]

$$F(q,\alpha) = L\frac{\sin\,(q\alpha L/2)}{q\alpha L/2}F_{cr}\,[\Delta\rho(r_c),q,\alpha] \tag{19}$$

The amplitude of the cross section of the molecules follows as

$$F_{cr}(\Delta\rho\,(r_c),q,\alpha) = \int_0^\infty \Delta\,\rho(r_c)\,J_0[qr_c(1-\alpha^2)^{1/2}]\,2\pi r_c\,dr_c \tag{20}$$

where $\Delta\rho(r_c)$ is the radial excess scattering length density and $J_0(x)$ is the Bessel function of zeroth order.

For $q \gg 2\pi/L$, the rod gives only a contribution to the measured intensity if $\vec{q}$ is perpendicular to the long axis [13], i.e., if $\alpha \simeq 0$. Thus, the intensity measured at higher scattering angles is directly related to the Hankel-transform of the excess electron density $\Delta\rho(r_c)$, which means that [13]

$$I_0(q) \approx L\frac{\pi}{q}F_{cr}(\Delta\rho\,(r_c),q_\perp)F^*_{cr}(\Delta\rho\,(r_c),q_\perp) \tag{21}$$

which, for polydisperse samples, can be rewritten as [24]

$$I_0(q) \approx L_n[\frac{\pi}{q}F_{cr}(\Delta\,\rho\,(r_c),q_\perp)F^*_{cr}(\Delta\rho\,(r_c),q_\perp)] \tag{22}$$

where L_n is the number-averaged contour length.

The scattering of the macroion can be modeled in terms of a real excess electron density $\Delta\rho_{rod}$. With a being the minimum approach of the macroion and the counterions, it follows that $\Delta\rho(r_c) = \Delta\rho_{rod}$ for all $r_c \le a$. For $r_c \ge a$, $\Delta\rho(r_c)$ is solely determined by the excess electron density of the counterions.

Let $n(r_c)$ denote the radial number density of the counterions. It follows that $\Delta\rho(r_c) = \Delta f_{ion} n(r_c)$ for $r_c \ge a$, where Δf_{ion} is the number of excess electrons of a single ion. As already discussed above, this quantity is given by combining Eqs. 1 and 3 [23, 24]

$$\Delta f_{ion} = f_0 - \rho_m V_{ion} + f' + \tilde{i}\cdot f'' \tag{23}$$

where V_{ion} is the volume of the counterion. The quantity ρ_m is the electron density of the solvent water which is independent of energy. The excess electron density to be introduced into Eq. 20 follows as

$$\Delta\rho(r_c) = \begin{cases} \Delta\rho_{rod} & 0 \le r_c \le a \\ n(r_c)\Delta f_{ion} & a \le r_c \le R_0 \\ 0 & r_c > R_0 \end{cases} \tag{24}$$

Here, R_0 denotes the cell radius introduced by the PB cell model (see below). $\Delta\rho(r_c)$ may therefore be split into a nonresonant term $\Delta\rho_0(r_c)$ and the resonant contributions of the counterions according to [23]:

$$\Delta\rho(r_c) = \Delta\rho_0(r_c) + n(r_c)f' + \tilde{i}\cdot n(r_c)f'' \tag{25}$$

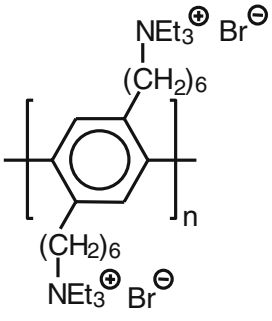

Fig. 3 Chemical structure of the rod-like polyelectrolyte used for the ASAXS study discussed here [25]

Insertion of Eq. 25 into Eqs. 20 and 18 leads to three terms that are related to the Hankel-transforms of the terms $\Delta\rho_0(r_c)$, $n(r_c)f'$, and $n(r_c)f''$, respectively [23]:

$$F(q,\alpha)F^*(q,\alpha) = \{L\frac{\sin(q\alpha L/2)}{q\alpha L/2}\}^2\{F_{cr}^2[\Delta\rho_0(r_c),q,\alpha] + 2f'F_{cr}[\Delta\rho_0(r_c),q,\alpha]F_{cr}[n(r_c),q,\alpha] + (f'^2+f''^2)F_{cr}^2[n(r_c),q,\alpha]\} \quad (26)$$

Equation 26 demonstrates that ASAXS leads to three partial intensities, as discussed above. In the following, these terms will be compared to the predictions of a meanfield approach, namely, the PB cell model.

PB cell model

The PB cell model treats the correlation of the counterions to a rod-like macroion in terms of a meanfield approach [8]. N rods are assumed to be confined in cells of radius R_0. The cell radius R_0 is determined by the condition $(N/V)\pi R_0^2 L = 1$. The distribution function $n(r_c)$ is then given by [41]

$$\frac{n(r_c)}{n(R_0)} = \{\frac{2|\beta|}{\kappa r_c\cos[\beta\ln(r_c/R_M)]}\}^2 \quad (27)$$

The integration constant β can be calculated by use of the condition [41]

$$\arctan(\frac{\xi-1}{\beta}) + \arctan(\frac{1}{\beta}) - \beta\ln(R_0/a) = 0 \quad (28)$$

for a set of parameters ξ, a, and R_0. The second constant R_M is given by

$$R_M = a\exp\{\frac{1}{\beta}\arctan(\frac{\xi-1}{\beta})\} \quad (29)$$

The screening constant $\kappa = 8\pi\lambda_B n(R_0) = 4(1+\beta^2)/R_0^2$ [41]. The distribution function $n(r_c)$ thus obtained for a given number density N/V can be used to calculate the respective scattering intensity according to Eqs. 18 and 26.

Because the polyelectrolyte shown in Fig. 1 has already been studied by conventional SAXS, all parameters can be taken from this work [16]. Hence, the charge parameter ξ is 3.3. The cell radius R_0 is determined from the number density of the rod-like polyelectrolyte. Subsequently, the integration constants β (see Eq. 28) and R_M (Eq. 29) are determined.

ASAXS: experimental problems

As mentioned in the "Introduction", ASAXS as a method has been known for a long time. Indeed, Stuhrmann was the first to apply this method to polyelectrolytes and to show the general feasibility [18]. However, ASAXS measurements are very demanding with regard to experimental accuracy. In the following, we shall enumerate briefly the main experimental problems of this method:

1. An important problem that needs to be taken into account is the resolution of the energy of the primary beam. Figure 1 demonstrates this by showing the profile of the primary beam together with $f'(E)$ and $f''(E)$. It is obvious that the variation of f', which is most pronounced in the immediate neighborhood of the edge, can only be used if the width of the primary beam is small enough. Moreover, a precise evaluation of the data requires that the finite width of the primary beam is taken into account by an appropriate average over f' and f'' [27]. This is done by weighing the respective scattering factors by the profile of the primary beam shifted to the respective energy. It leads to the effective scattering factors f'_{eff} and $''_{eff}$, which differ from f' and f'' in the immediate vicinity of the edge [25, 27].
2. The absorption edge must be localized with the highest precision possible. ASAXS rests mainly on the variation of f' with the energy E of the incident beam. Hence, precise measurements of the absorption may be used to find the exact position of the edge and to detect small shifts of the monochromator of the instrument [25, 27].
3. The parasitic background caused by the scattering of water and by fluorescence must be subtracted properly. Fluorescence comes into play even below the edge because of the finite width of the primary beam (see Fig. 3). In the immediate neighborhood of the edge, a part of the energy of the primary beam will be above the edge and hence cause fluorescence [27].
4. Absolute intensities must be determined with utmost precision. Equation 26 demonstrates that the entire ASAXS effect consists of a small decrease of the measured intensity when approaching the absorption edge. Any error in determining the absolute intensity would render the evaluation of the data impossible. Figure 4 demonstrates this problem by showing the net effect of ASAXS. Here, the absolute intensities measured at four different energies are shown [25]. There is a small but measurable shift that can be evaluated if the calibration has been done accurately [25, 27].

These problems have been solved for the rod-like polyelectrolytes under consideration here [27], for spherical polyelectrolytes [27], and for flexible polyelectrolytes in presence of strontium ions [28]. For details of the procedures, the reader is referred to these original papers.

Partial intensities determined by ASAXS

Equation 26 shows that ASAXS leads to three partial intensities, namely, the first term which contains the nonresonant scattering, the cross term, and the third term that is solely due to the resonantly scattering units. The latter partial intensity, named the self-term, is the most interesting result because it is the scattering intensity of the cloud of counterions only. This term is small as compared to the other partial intensities and was disregarded in previous ASAXS studies of polyelectrolytes [23, 26].

Subtracting two large terms to give a small difference is a numerically ill-posed problem. Here, we proceed by a different scheme for the general treatment of the ASAXS data that is applicable to any system under consideration: Eq. 26 is a quadratic form in terms of the scattering factor f' if f'' is disregarded. This approximation is certainly justified for data below the edge, where f'' is rather small indeed (see Fig. 1). A detailed study of this problem has demonstrated that the variation of f'' is practically inconsequential even above the edge [25, 27]. This is due to the finite error in defining the position of the edge and other experimental uncertainties [25]. Hence, for each q value, the set of all scattering curves measured below and above the edge were plotted in Fig. 5 as the function of solely f'_{eff} . This plot shows the accuracy of the present decomposition. The plot can hence be used to determine the three partial intensities given in Eq. 26.

Figure 6 displays the three partial intensities. Here, the upper curves (circles) correspond to the SAXS intensity measured by a conventional SAXS experiment far below the edge. The lowermost curve (triangles) is the self-term of Eq. 26, and the curve in between marks the cross-term (squares). As expected from previous model calculations, the intensities exhibit a very similar dependence on q [23]. Note that the self-term, which is much smaller than the nonresonant term or the cross term, can be obtained up to $q = 2.5\ nm^{-1}$. As mentioned above, this term provides the most valuable information of the ASAXS experiment. It refers to the scattering intensity that would result from a system in which the macroion is totally matched.

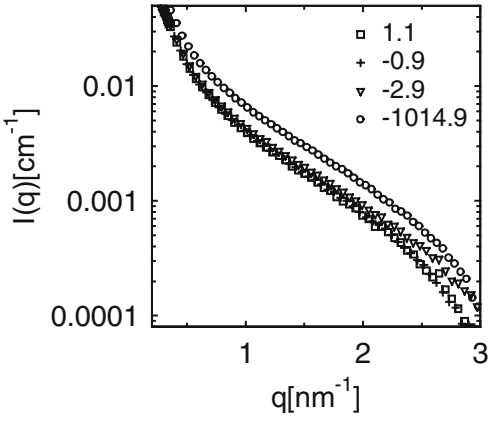

Fig. 4 ASAXS intensities corrected for the fluorescence and the parasitic background by the solvent water. The difference of the energy of the incident beam to the edge is indicated in the graph

Comparison with the PB cell model

The three partial intensities displayed in Fig. 6 can now serve for an unambiguous test of the cell model described in the "Theory" section. The comparison with the cell model can be done as described in great detail recently [24]. With the distribution $n(r_c)$, the partial scattering intensities in Eq. 26 can now be calculated and compared to the experimental data shown in Fig. 6.

The contrast parameters entering into this comparison have been determined recently for the system under consideration here (see Fig. 1). The contrast Δf_{ion} of the Br^- counterions was determined from their respective crystallographic radii. Hence, as already discussed in previous papers [16, 23, 24], the hydration shell of the ion is treated as bulk water. This may induce a small error if Δf_{ion} is small. The value calculated in this way for Br^- is $\Delta f_{ion} = 26\ e^-/ion$. For the contrast of the macroion, we used the value $\Delta\rho_{rod} = 25\ e^-/nm^3$ [16].

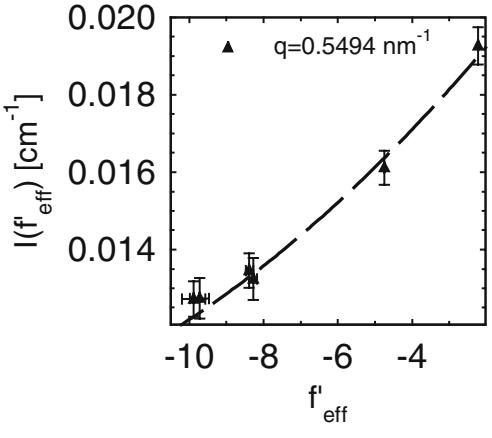

Fig. 5 Decomposition of the ASAXS intensities measured at different energies of the incident beam according to Eq. 26. The intensities measured at a q value given in the graph are plotted against the effective real part f'_{eff} of the scattering factor (cf. the discussion of Fig. 3). The *dashed line* shows the fit according to Eq. 26 if $''_{eff}$ is disregarded. Taken from Patel et al. [25]

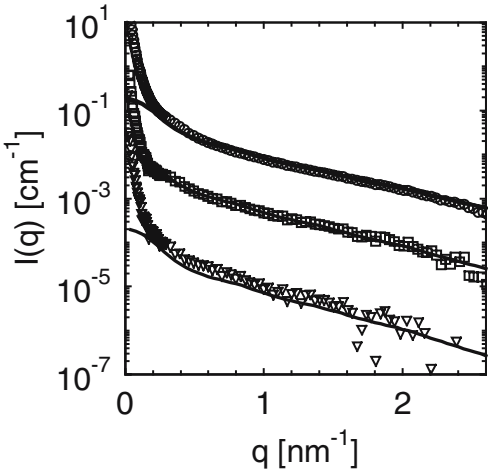

Fig. 6 The partial intensities obtained by ASAXS are plotted against q and compared to the prediction of the cell model. The *upper curve* is the first term in Eq. 26 and refers to the intensity obtained far below the edge. The *lowermost term* is the self-term that solely refers to the scattering contribution of the counterions (third term of Eq. 26). The *middle curve* is the cross-term (second term of Eq. 26). The *solid lines* mark the prediction of the cell model. Taken from Patel et al. [25]

The solid lines in Fig. 6 show this comparison [25]. Figure 6 shows that good agreement is reached for all three partial intensities. All ratios between the intensities, as well as their dependence on q , are captured by the cell model. Only the self-term is slightly underestimated, but the small differences seen in Fig. 6 are hardly beyond the experimental uncertainty. All parameters are either fixed or have been taken from a previous analysis as $\Delta\rho_{rod}$. Moreover, as is obvious from Eq. 26, the self-term is not dependent on any contrast and is thus model-independent.

Figure 6 demonstrates that the PB approach, that is, a meanfield theory, yields a satisfactory description of all partial scattering intensities available by ASAXS. This is to be expected for the cross-term that is solely related to the meanfield distribution of the counterions. The third term, on the other hand, contains a contribution that is sensitive to fluctuations, that is, on deviations of the average distribution. The good agreement of this term with the PB theory reveals that fluctuations must be small. This in turn leads to the conclusion that there must be a strong correlation of the counterions to the macroion. The strong electric field of the highly charged rod-like ion obviously suppresses the fluctuations, and the meanfield approach provides a sufficient description.

Conclusion

The present survey has demonstrated the power of the ASAXS study for the study of rod-like polyelectrolytes in aqueous solutions. Most importantly, ASAXS gives the intensity contribution that is solely due to the counterions (third term of Eq. 26). Moreover, the comparison between the different partial intensities leads to a quantitative analysis of the correlations of the counterions to the macroion. Hence, ASAXS data may be used to detect contributions to the scattering intensity that are due to fluctuations. In this way, ASAXS furnishes data that are not available by a conventional scattering experiment.

Acknowledgements Financial support by the Deutsche Forschungsgemeinschaft, Sonderforschungsbereich 481, Bayreuth; by the EU, Project POLYAMPHI; and by the Fonds der Chemischen Industrie, is gratefully acknowledged.

References

1. Mandel M (1988) In: Mark FH, Bikales NM, Overberger CG, Menges G (eds) Encyclopedia of polymer science and engineering, vol 11, 2nd edn. Wiley, New York, p 739
2. Schmitz KS (1993) Macroions in solution and colloid suspension. VCH, New York
3. Hansen JP, Löwen H (2000) Annu Rev Phys Chem 51:209
4. Belloni L (2000) J Phys Condens Matter 12:R549
5. Dijkstra M (2001) Curr Opin Colloid Interface Sci 6:372
6. Löwen H, Allahyarov E, Likos CN, Blaak R, Dzubiella J, Jusufi A, Hoffmann N, Harreis HM (2003) Phys A Math Gen 36:5827
7. Manning G (1972) Annu Rev Phys Chem 23:117 (and further references cited therein)
8. Deserno M, Holm Ch, Blaul J, Ballauff M, Rehahn M (2001) Eur Phys J E 5:97
9. Jusufi A, Likos CN, Löwen H (2002) Phys Rev Lett 88:18301
10. Jusufi A, Likos CN, Löwen H (2002) J Chem Phys 116:11011
11. Jusufi A, Likos CN, Ballauff M (2004) Colloid Polym Sci 282:910
12. Glatter O, Kratky O (eds) (1982) Small-angle X-ray scattering. Academic, London
13. Porod G (1982) In: Glatter O, Kratky O (eds) Small-angle X-ray scattering. Academic, London
14. Wu CF, Chen SH, Shih LB, Lin JS (1988) Phys Rev Lett 61:645
15. Chang SL, Chen SH, Rill RL, Lin JS (1990) J Phys Chem 94:8025
16. Guilleaume B, Blaul J, Wittemann M, Rehahn M, Ballauff M (2000) J Cond Matter 12:A245
17. Zakharova SS, Engelhaaf S, Bhuiyan LB, Outhwaite CW, Bratko D, van der Maarel JRC (1999) J Chem Phys 111:10706 (and further references cited therein)
18. Stuhrmann HB (1985) Adv Polym Sci 67:123
19. Stuhrmann HB, Goerigk G, Munk B (1991) In: Ebashi S, Koch M, Rubenstein E (eds) Handbook of synchrotron radiation, vol 4, chapter 17. Elsevier, Amsterdam, p 557
20. Guinier A, Fournet G (1955) Small-angle scattering of X-rays. Wiley, New York

21. Henke BL, Gullikson EM, Davis JC (1993) At Data Nucl Data Tables 54:181
22. Brennan S, Cowan PL (1992) Rev Sci Instrum 63:850
23. Guilleaume B, Ballauff M, Goerigk G, Wittemann M, Rehahn M (2001) Colloid Polym Sci 279:829
24. Guilleaume B, Blaul J, Ballauff M, Wittemann M, Rehahn M, Goerigk G (2002) Eur Phys J E 8:299
25. Patel M, Rosenfeldt S, Dingenouts N, Pontoni D, Narayanan T, Ballauff M (2004) Phys Chem Chem Phys 6:2962
26. Das R, Mills TT, Kwok LW, Maskel GS, Millett IS, Doniach S, Finkelstein KD, Herschlag D, Pollack L (2003) Phys Rev Lett 90:188103
27. Dingenouts N, Patel M, Rosenfeldt S, Pontoni D, Narayanan T, Ballauff M (2004) Macromolecules 37:8152
28. Goerigk G, Schweins R, Huber K, Ballauff M (2004) Europhys Lett 66:331
29. Jusufi A, Ballauff M (2006) Macromol Theory Simul 15:193
30. Jusufi A (2006) J Chem Phys 124:044908
31. Angermund K, Buhl M, Endruschat U, Mauschick FT, Mortel R, Myott R, Tesche B, Waldofner N, Bonnemann H, Koehl G, Modrow H, Hormes J, Dinjus E, Gassner F, Haubold HG, Vad T, Kaupp M (2003) J Phys Chem B 107:7507
32. Goerigk G, Haubold HG, Lyon O, Simon JP (2003) J Appl Crystallogr 36:425
33. Brumberger H, Hagrman D, Goodisman J, Finkestein KD (2004) J Appl Crystallogr 38:147
34. Tatchev D, Goerigk G, Valova E, Dille J, Kranold R, Armyanov S, Delplancke JL (2005) J Appl Crystallogr 38:787
35. Luis AS, Prado A, Goerigk G, Ponce ML, Garamus VM, Wittich H, Willumeit R, Schulte K, Nunes (2005) J Polym Sci B Polym Phys 43:2981 (and further references cited therein)
36. Hansen JP, McDonald IR (1986) Theory of simple liquids. Academic, London
37. Harreis HM, Likos CN, Ballauff M (2003) J Chem Phys 118:1979
38. Fuoss RM, Katchalsky A, Lifson S (1951) Proc Natl Acad Sci USA 37:579
39. Alfrey T, Berg PW, Morawetz H (1951) J Polym Sci 7:543
40. Katchalsky A (1971) Pure Appl Chem 26:327
41. Le Bret M, Zimm B (1984) Biopolymers 2:287